

Lifetime-Limited Linewidth Measurements of the 3C and 3D Soft X-ray Transitions in Ni XIX

Chintan Shah,^{1,2,3,*} Steffen Kühn,^{2,4} Sonja Bernitt,^{2,5,6,7} René Steinbrügge,⁸ Moto Togawa,^{2,4} Lukas Berger,² Jens Buck,⁹ Moritz Hoesch,⁸ Jörn Selmann,⁸ Mikhail G. Kozlov,¹⁰ Sergey G. Porsev,¹¹ Ming Feng Gu,¹² F. Scott Porter,¹ Thomas Pfeifer,² Maurice A. Leutenegger,¹ Charles Cheung,¹¹ Marianna S. Safronova,¹¹ and José R. Crespo López-Urrutia²

¹NASA/Goddard Space Flight Center, 8800 Greenbelt Rd, Greenbelt, MD 20771, USA

²Max-Planck-Institut für Kernphysik, Saupfercheckweg 1, 69117 Heidelberg, Germany

³Department of Physics and Astronomy, Johns Hopkins University, Baltimore, MD 21218, USA

⁴Heidelberg Graduate School of Fundamental Physics, Ruprecht-Karls-Universität Heidelberg, Im Neuenheimer Feld 226, 69120 Heidelberg, Germany

⁵Institut für Optik und Quantenelektronik, Friedrich-Schiller-Universität Jena, Max-Wien-Platz 1, 07743 Jena, Germany

⁶Helmholtz-Institut Jena, Fröbelstieg 3, 07743 Jena, Germany

⁷GSI Helmholtzzentrum für Schwerionenforschung, Planckstraße 1, 64291 Darmstadt, Germany

⁸Deutsches Elektronen-Synchrotron DESY, Notkestraße 85, 22607 Hamburg, Germany

⁹Institut für Experimentelle und Angewandte Physik (IEAP),

Christian-Albrechts-Universität zu Kiel, Leibnizstr. 11-19, 24098 Kiel, Germany

¹⁰St. Petersburg Electrotechnical University "LETI", Prof. Popov Str. 5, St. Petersburg, 197376, Russia

¹¹Department of Physics and Astronomy, University of Delaware, Newark, Delaware 19716, USA

¹²Space Science Laboratory, University of California, Berkeley, CA 94720, USA

(Dated: April 24, 2024)

We used the monochromatic soft X-ray beamline P04 at the synchrotron-radiation facility PETRA III to resonantly excite the strongest $2p-3d$ transitions in neon-like Ni XIX ions, $[2p^6]_{J=0} \rightarrow [(2p^5)_{1/2} 3d_{3/2}]_{J=1}$ and $[2p^6]_{J=0} \rightarrow [(2p^5)_{3/2} 3d_{5/2}]_{J=1}$, respectively dubbed 3C and 3D, achieving a resolving power of 15,000 and signal-to-background ratio of 30. We obtain their natural linewidths, with an accuracy of better than 10%, as well as the oscillator-strength ratio $f(3C)/f(3D) = 2.51(11)$ from analysis of the resonant fluorescence spectra. These results agree with those of previous experiments, earlier predictions, and our own advanced calculations.

I. INTRODUCTION

Because of their closed-shell $n = 2$ ground-state configuration, neon-like ions are prevalent in plasmas across a broad range of temperatures. Their strong spectral lines provide a wealth of diagnostic capabilities, including temperature, density, optical depth, and ultraviolet field intensity. Their spectra were extensively studied in investigations of the Sun and other celestial bodies with the *Chandra* and *XMM-Newton* observatories [1–16]. The spectrum of Fe XVII is the most commonly studied in the soft x-ray band due to the high cosmic abundance of iron and the easily accessible energy of its $n = 2-3$ transitions, while Ni XIX is the second-most abundant such species.

Despite the apparent simplicity of their electronic structure, systematic discrepancies in the intensities of their strongest emission lines were long noted between theory, astrophysical observations, and laboratory measurements (see [17] and references therein). Recently, we solved in Ne-like Fe XVII a problem that persisted for several decades: the oscillator-strength ratio between its $2p-3d$ resonance (3C: $[2p^6]_{J=0} \rightarrow [(2p^5)_{1/2} 3d_{3/2}]_{J=1}$) and intercombination (3D: $[2p^6]_{J=0} \rightarrow [(2p^5)_{3/2} 3d_{5/2}]_{J=1}$) lines consistently deviated from predictions [17]. Previous experiments on this topic had suffered from both known and unexpected systematic uncertainties [18–30]. Our resonant excitation scheme using synchrotron radiation with much increased resolution and

signal-to-noise ratio finally brought experiment and theory into agreement [31].

In most measurements of Fe XVII, an inner-shell satellite from Na-like ions (line C: $[2p^6 3s]_{J=1/2} \rightarrow [(2p^5)_{1/2} (3s 3d)_{5/2}]_{J=3/2}$) blended with the Ne-like line 3D, leading to potential systematic errors in the line ratio [20]. Experiments in which 3C and 3D were excited by electron impact, and which had sufficient spectral resolving power to detect other lines of Na-like Fe, allowed correction of the strength of line 3D for contamination from line C, as well as optimization of the experimental conditions to minimize production of that undesired charge state. Photoexcitation measurements suffer from a second, subtler effect: the strong autoionizing branch of the upper level of line C continuously feeds the Ne-like ground state. In these experiments with insufficient resolution to split lines C and 3D, the resulting population transfer severely affected the apparent 3C/3D line-intensity ratio [32]. Only the most recent photoexcitation measurements mentioned above [31], with a resolving power of 20,000, could reduce this detrimental transfer effects, reducing the effective overlap between lines C and 3D to less than 1%.

Another approach to understanding issues in the 3C/3D ratio in Ne-like iron is to study the same ratio along the iso-electronic sequence as a function of atomic number Z . This has two advantages: first, any systematic errors peculiar to a single experiment are revealed as outliers; second, the scaling with atomic number of any deviation from predictions can guide future theoretical investigations. 3C/3D ratios for Ne-like ions ranging from Cr XV to Kr XXVII ($Z = 24-36$) were measured at the Lawrence Livermore National Labora-

* chintan.shah@mpi-hd.mpg.de

tory (LLNL) using an electron beam ion trap (EBIT) equipped with crystal spectrometers [33], showing systematic departures from theory from 10–20%. Extending our photoexcitation experiment to Ne-like Ni, where the lines 3D and C are much further apart than in Fe XVII, would fully suppress the undesired 3D-C overlap. This, the closeness of nickel to iron in Z , and the astrophysical importance of nickel motivated our present measurement in Ne-like Ni XIX ions. Because of the lower chemical abundance of nickel, its L-shell lines are weaker than those of iron in astrophysical sources. Ni XIX is nevertheless extremely useful for understanding the spectra of the solar and stellar coronae [34, 35] and for determinations of abundances, as well as plasma temperature and density [36]. In many high-energy-density plasmas [37–39], 3C and 3D are stronger than the other L-shell transitions and affect the Rosseland mean opacity, for which recent studies at temperatures akin to stellar interiors disagreed by 10–20% from models for Ni [40]. Thus, an experimental benchmark is also needed for validating the underlying atomic data in opacity models, and could help clarifying the iron-opacity problem [41, 42].

Ability of atomic methods to accurately predict core parameters, such as transition energies, transition rates, and subsequently derived values, e.g., collisional cross sections, critically depends on the benchmark tests where predicted values are compared against the experiment. The most readily accessible properties are transition energies, where most accurate experimental data can be obtained. Comparing theoretical and experimental energies is an excellent start on testing the atomic methods, as discrepancies in the energies immediately point to the method deficiencies. However, the agreement of the energies does not predict a high level of accuracy of all the other properties. Energy comparisons do not account for different dependence of the atomic properties on the distance from the nucleus, additional correlation corrections specific to the transition operators, and subtler effects of the configuration mixing. Thus, to fully validate atomic structure calculations, experiments measuring natural linewidths and lifetimes are essential.

Lifetimes of excited HCI from the optical to the X-ray domain have been measured from decades using among others accelerators, storage rings, and electron beam ion traps (EBIT). At accelerators, beam-foil techniques cover a few ns to hundreds of fs range [43–45], relying on spatially resolving X-ray emission following the passage of a fast ion through a thin foil. However, complexities arising from multiple excitations and charge-state distribution limits in general the accuracy of such data. Kingdon traps were also used for some lifetime measurements on ions [46–48]. Storage rings have allowed for many accurate lifetime studies up to the range of seconds, e. g. in Refs. [49–59] upon injection of excited HCI from external sources [60, 61], and in the optical range also using re-excitation of the circulating ions with lasers [62–64]. At EBITs, lifetimes ranging from ms down to ns are accurately measured by monitoring the decay of fluorescence after pulsed excitation, yielding uncertainties as low as 0.15% [65–69]. For the fs range, natural linewidths were accessed with high-resolution crystal spectrometers using stan-

dalone EBITs [39], or combined with synchrotron-radiation excitation [70–72]. Yet, modeling line profiles remains difficult, substantially limiting the achievable accuracy.

In this Letter, we present resonant photoexcitation of trapped Ni XIX ions at the monochromator beamline P04 at the PETRA III facility, with a focus on the two strong emission lines 3C and 3D. Several experimental improvements raised our resolving power to $\sim 15,000$ and the signal-to-noise ratio to ~ 30 , enabling an accurate determination of the 3C/3D oscillator-strength ratio with approximate statistical and total uncertainties of 0.5% and 4.5%, respectively. Our observed line shapes yield the absolute natural linewidths, lifetimes, and oscillator strengths for 3C and 3D lines with an accuracy better than 10%. All measurements agree well with our new predictions.

II. MEASUREMENTS AND ANALYSIS

We carried out the experiment with PolarX-EBIT [73], which is dedicated to the study of interactions of trapped highly charged ions (HCI) with photons from external sources, at the P04 beamline [74] of the PETRA III synchrotron-radiation facility. An off-axis electron gun emits a nearly mono-energetic electron beam that is compressed to a diameter of less than $100\ \mu\text{m}$ by an 870 mT magnetic field generated by an array of permanent magnets. Precursor atoms of Ni were brought in as a tenuous molecular beam of nickelocene (bis(cyclopentadienyl)nickel (C_5H_5)₂Ni) injected into the trap region through a two-stage differential pumping system. Successive electron impacts ionize Ni atoms to the charge state of choice. The ions are confined radially by the negative space-charge potential produced by the ~ 5.5 mA and ~ 1.1 keV electron beam, and axially by the ~ 10 V potential difference given to the drift tubes before and after the central one. At the soft X-ray beamline P04, an APPLE II undulator generates circularly polarized photons which are monochromatized with a variable line-spacing platinum-coated 1200 l/mm grating [74]. A Kirkpatrick-Baez (KB) mirror system refocuses the photon beam at the position of the PolarX trap region a few meters downstream. The focus diameter there is slightly smaller than the ion cloud itself, which is approximately 200 micrometers broad. The photon beam enters PolarX from the side where the off-axis electron gun is mounted, and propagates along its longitudinal axis, defined by the magnetic field and the narrow electron beam that it guides and compresses. The photon beam is focused for maximum overlap onto the approximately 16 mm long cloud of Ni ions confined within the central trap electrode. Upon excitation, the resulting fluorescence is detected by two identical silicon drift detectors (SDD) with a resolving power of 10% at 1 keV mounted at right angles to the photon beam on the top and the side of the trapping region. After passing the trap region, the photon beam exits unimpeded PolarX through its collector, and enters a downstream beamline, where we measure its intensity.

For production of Ni XIX ions, the electron-beam energy must exceed 607 eV. This also leads to electron-impact-

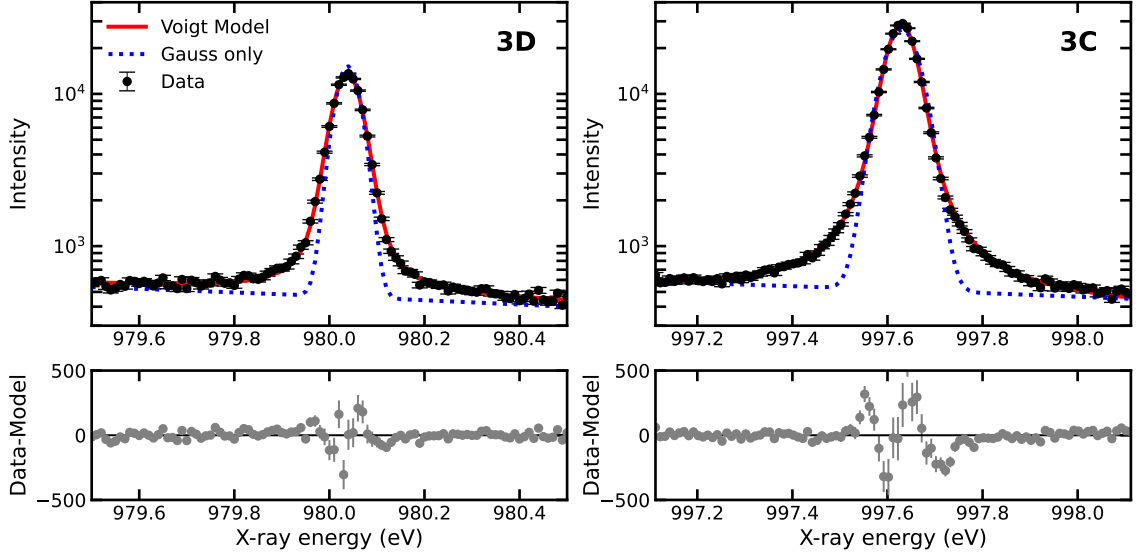


FIG. 1. Summed fluorescence yield of the soft X-ray transitions 3C and 3D of Ni XIX versus excitation photon energy. Fitted Voigt profiles shown in red with their residuals in the bottom panels. For comparison, blue curves show only the Gaussian component of the model, normalized to the same peak intensity.

induced fluorescence from dielectronic recombination as well as resonant and direct excitation [26] that is much stronger than the sought-after photoexcitation signal. We address this by periodically switching within a few microseconds the electron-beam energy between two optimized values, breeding for 200 ms Ni XIX ions at 1090 eV and detecting for 50 ms their fluorescence at 280 eV. This suppresses in-band background photons induced by electron-impact processes, resulting in a cleaner photoexcitation signal [31]. The residual background results from electron impact production of few-hundred-eV photons which partly blend in the SDD with 3C and 3D due to its finite energy resolution and the width of the region of interest. Optimization of the ion-breeding duty cycle allowed us to further narrow the monochromator exit slit width to 25 μm while keeping a strong fluorescence signal and achieving a robust signal-to-background ratio close to ~ 30 . The narrow slit allows the resolving power of the monochromator to reach values up to 15,000 for the Ni XIX 3C and 3D transitions.

We scanned a range of ± 500 meV around the known centroid energies [36, 75] in 100 steps of 10 meV each, while integrating the photoexcitation signal for ~ 6 seconds at each monochromator step to ensure sufficient statistics in the line wings. To generate the spectrum, X-rays detected within a given region of interest centered on the expected energies of 3C and 3D were summed and projected onto the monochromator energy axis. These scans were repeated 20 times, and the resulting (summed) data is shown in Fig. 1. Each individual scan is fitted with a Voigt profile, a convolution of Gaussian and Lorentzian distributions. The Gaussian component arises from the Doppler width of the trapped ions and the apparatus profile of the monochromator [76]. Meanwhile, the Lorentzian component, as explained in detail in our previous work [31, 77], results not only from the natural linewidth of

the transitions but also from a pseudo-Lorentzian instrumental component caused by X-ray diffraction at beamline components [78]. Total intensities were determined from the area under the curve, derived through a maximum-likelihood fit of Voigt profiles using the Cash statistic [79, 80]. Furthermore, 3C and 3D intensities were corrected for the presence of a 500-nm Al filter in front of SDDs, and normalized by the photon flux measured downstream of the EBIT with a calibrated photodiode, which together increase the ratio by 0.5%. Given that the intensity of the 3C and 3D transitions excited by the monochromatic X-ray beam is directly proportional to the oscillator strength of each transition [27, 81], we derived an oscillator strength ratio of 2.51(2) from the measured intensities. We note that the inner-shell satellite C of the Na-like ion, previously a major source of systematic uncertainties in many experiments on Fe XVII, does not affect the Ni XIX 3C/3D line ratio. This is primarily because line C is clearly separated from line 3D, falling well outside the scan range we used. From our low-resolution measurement with a 1-mm exit slit, we determined the difference $\Delta E_{3D-C} \approx 2.4$ eV.

The measured line ratio could be affected by periodic fluctuations of the actual photon energy around its nominal value, stemming from incorrect interpolation tables for the grating and mirror angular encoders [78, 96] of the monochromator, as discussed in our previous work [31, 77, 97]. To avoid this issue in subsequent works, we simultaneously measured a proxy for the fluctuations of the true photon energy with a photoelectron-energy spectrometer (ASPHERE) [98]. Unfortunately, this instrument was not available during the present measurements, but in follow-up campaigns [77] we found with it oscillating differences between nominal and true photon energy of up to $\approx \pm 70$ meV in the Ni XIX 3C and 3D scan range. We simulated such monochromator fluctuations with mock 3C and 3D Voigt profiles, resulting in system-

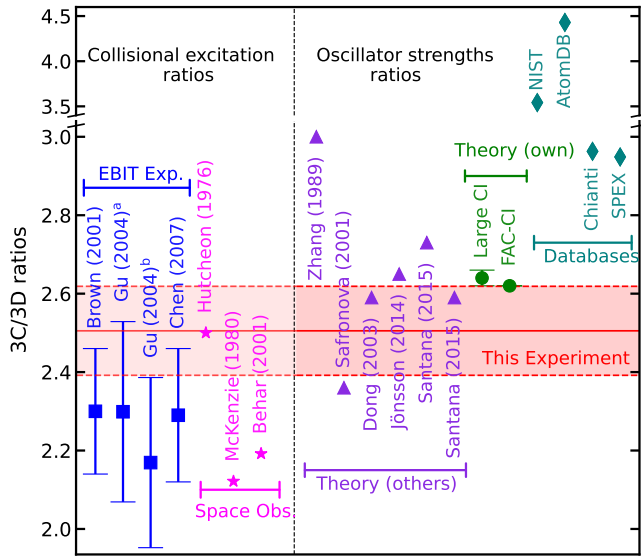


FIG. 2. Present experimental Ni XIX 3C/3D oscillator-strength ratio in comparison with collision-strength ratios measured in prior EBIT experiments: with crystal spectrometer Brown *et al.* [20], with grating spectrometer Gu *et al.* [82]^a, and microcalorimeters in Gu *et al.* [82]^b and Chen *et al.* [83], solar observations [35, 84], and Chandra studies of Capella [7]. Our measured oscillator-strength ratio is also compared with earlier theoretical studies [85–89], our own predictions [90, 91], and commonly used spectral plasma models and databases [92–95].

atic uncertainties of approximately 3% in the 3C/3D intensity ratio. A slight line profile asymmetry caused by X-ray diffraction at beamline components was quantified by fitting with skewed Voigt profiles, showing changes in the ratio of less than 0.5%. We observed scan-to-scan variations in the amplitudes of 3C and 3D of $\sim 3\%$ which are not attributable to any known cause, and which we therefore take as a term in our systematic error budget. All above systematic uncertainties, including the $\sim 0.1\%$ uncertainty in the 3C/3D ratio arising from a 10% uncertainty in the thickness of the 500-nm Al optical filter, have been taken into account in the final error budget for the inferred oscillator-strength ratio, namely $f(3C/3D) = 2.51(2)_{\text{stat}}(11)_{\text{sys}}$, as displayed in Fig. 2. Please note that the circular polarization of the photon beam does not influence the ratio, as both transitions 3C and 3D have identical angular emission characteristics (see Appendix A in Ref. [72]).

To determine the natural linewidths of 3C and 3D, we used the Gaussian and Lorentzian widths extracted through Voigt fits to twenty scans of 3C and 3D. While Gaussian widths of approximately 50 meV for 3C and 3D were consistent with the experimental conditions, the extracted Lorentzian widths of ~ 30 and ~ 17 meV for 3C and 3D transitions, respectively, were clearly larger than expected from theory. We attribute this discrepancy to an additional pseudo-Lorentzian component induced by X-ray diffraction at beamline components [78, 96] that artificially raises the apparent Lorentzian linewidth of observed transitions, as shown

in our previous work [31]. We checked this here by measuring the $K\alpha$, $K\beta$, and $K\gamma$ X-ray transitions from helium-like F VII and Ne IX several times. Their theoretical natural linewidths were taken from the NIST Atomic Spectral Database (ASD) [92, 99, 100], and we assigned them a conservative 10% uncertainty [36]. As Lorentzian contributions add linearly, in contrast to the quadratic addition of Gaussian widths, we subtracted the theoretical natural linewidths from the Lorentzian linewidths inferred from the measurements. We noticed an increase in the pseudo-Lorentzian beamline component dependent on the monochromator energy, which we model empirically as a quadratic function, determining the beamline Lorentzian contribution at 3D and 3C line energies to be 10.0(1.0) and 10.3(1.1) meV, respectively. We also derived beamline Lorentzian contributions of 7.2(5) meV and 7.4(5) meV at Fe XVII 3D and 3C energies, respectively, and upon comparison with the 7.0(3) meV obtained in our earlier work [31], which relied exclusively on the single F VIII $K\beta$ line, we find reasonably good agreement between the present and Kühn *et al.* [31].

To derive the natural linewidths of Ni XIX 3C and 3D, we subtracted the pseudo-Lorentzian instrumental component from the Lorentzian widths obtained from Voigt fits to each scan of both lines. The determined natural linewidths were 19.8(1.2) and 7.1(1.0) meV for 3C and 3D, respectively, indicated as "Method 1" in Tab. I and in Fig. 3. Their uncertainties include the statistical error on individual widths obtained from the fit, and systematic uncertainties from asymmetric line shapes (2%), monochromator energy fluctuations at 3C (2.2%) and 3D (2.3%) and at the helium-like K-shell reference transitions of helium-like F and Ne ions (6%).

Alternatively, we can use the following equations to determine the individual natural linewidths of 3C and 3D using the *difference* in their uncalibrated Lorentzian widths, as shown in Kühn *et al.* [31]:

$$\Gamma_{3C} = \frac{\Delta\Gamma_{3C-3D}}{1 - f(\frac{3D}{3C})E(\frac{3D}{3C})^2}, \text{ and } \Gamma_{3D} = \frac{\Delta\Gamma_{3C-3D}}{f(\frac{3C}{3D})E(\frac{3C}{3D})^2 - 1}.$$

However, in this second method, we have assumed that the pseudo-Lorentzian contribution from the beamline is similar for both 3C and 3D lines, as in Kühn *et al.* [30]. This allows the subtraction of Lorentzian widths obtained directly from the 3C and 3D Voigt fits ($\Delta\Gamma_{3C-3D} = 13.0(1.4)$ meV). By utilizing this difference along with the measured $f(3C/3D)$ oscillator-strength ratio in the present work and the transition-energy $E(3C/3D)$ ratio measured in [75] in the above equations, we determined the natural linewidths of 3C and 3D to

TABLE I. Natural linewidths (Γ^{exp}) for 3C and 3D of Ni XIX in meV, as determined using two different methods, as well as their mean. Pearson correlation coefficients $\rho_{3C,3D}$ for Γ_{3C} and Γ_{3D} are also listed.

Natural linewidths (Γ^{exp})	Line 3C (meV)	Line 3D (meV)	$\rho_{3C,3D}$
Method 1	19.8 ± 1.2	7.1 ± 1.0	0.10
Method 2	21.2 ± 2.7	8.3 ± 1.2	0.94
Mean (equal weights)	20.5 ± 1.7	7.7 ± 0.7	0.63

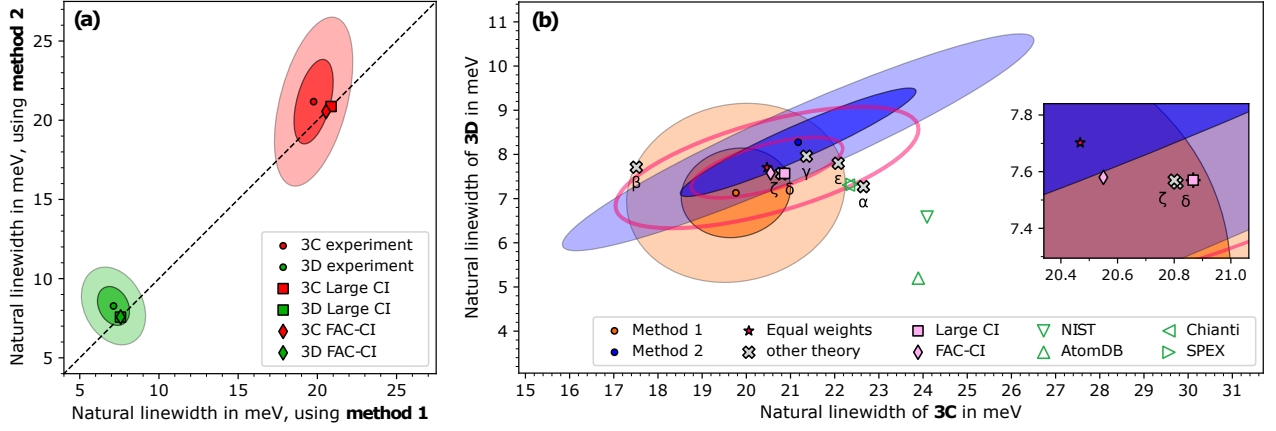


FIG. 3. (a) Results for the natural linewidths of 3C (red) and 3D (green) for Ni XIX analyzed by two different methods, with ellipses displaying their one- and two-sigma experimental uncertainties. The dashed diagonal line marks where both methods coincide. Predictions from large-CI (squares) and FAC-CI (diamonds) are shown. (b): Natural line widths inferred for 3C and 3D. Ellipses: one- and two-sigma experimental uncertainties for method 1 (orange) and method 2 (blue), as well as for their mean with equal weights (magenta star and lines). Symbols: Predictions from (pink square) our large-CI, (pink diamond) our FAC-CI, other calculations (grey crosses; α (DW): Zhang and Sampson [85], β (MBPT): Safronova *et al.* [86], γ (MCDF): Dong *et al.* [87], δ (CI): Jönsson *et al.* [88], and ε (CI), ζ (MBPT): Santana *et al.* [89].

be 21.2(2.7) and 8.3(1.2) meV, respectively. The final errors in this method (Method 2) account for Voigt fit statistical errors on individual widths, asymmetric line shapes (2%), effects of monochromator energy fluctuations on 3C (2.2%) and 3D (2.3%), and on $\Delta\Gamma_{3C-3D}$ (5%), in addition to the uncertainty in $f(3C/3D)$ from this work and the $E(3C/3D)$ uncertainty from [75].

In both methods, we propagated uncertainties and covariances using Monte-Carlo methods, obtaining final natural linewidths values for 3C and 3D lines as unweighted means of all 20 individual measurements. A comparison of the results of both methods is displayed in Fig. 3(a). It shows that results for both linewidths are largely uncorrelated in Method 1, as it is less prone to systematics, while Method 2 exhibits a Pearson correlation coefficient close to one for both linewidths, indicating high correlation and greater susceptibility to systematics arising from amplitude ratios, energy ratios, and the assumption of similar beamline components. As an unbiased compromise, we choose their unweighted mean values as our final results presented in Tab. I and shown as magenta ellipses in Fig. 3(b).

III. RESULTS AND DISCUSSIONS

Figure 2 compares our results with earlier experimental data, observations, and predictions. Our own calculations using large-scale configuration interaction (large-CI) [90] and FAC-CI [91] methods, both accounting for the relativistic Breit interaction and quantum electrodynamics (QED) effects, yield an oscillator-strength ratio which agrees with our experiment within the uncertainties. Details of large-CI computations are given in Appendix . Additional comparisons with other theoretical values from the literature showed typical departures within a $1-2\sigma$ range, with the largest one from Zhang

and Sampson [85].

Three laboratory measurements of the 3C/3D intensity ratio of Ni XIX based on electron-impact excitation (EIE) were reported [33, 36, 83]. The collisional excitation ratios from all three previous experiments span 1.90–2.35, slightly lower than the oscillator strength ratio measured in our experiment, but all four experiments are mutually consistent within uncertainties. Observations of the solar corona [35, 84] and Capella [7] show some scatter in the 3C/3D ratio, but in the absence of uncertainty estimates we cannot quantify the level of agreement with laboratory measurements.

Figure 3 (a) shows a comparison between measured 3C and 3D natural linewidths obtained using two different methods, which agree (see dashed diagonal lines) with each other and our predictions. Both our calculations using large-CI and FAC-CI methods agree within the 1σ uncertainty of our experimental results. As can be seen in Figure 3 (b), the other older calculations from Zhang and Sampson [85] and Safronova *et al.* [86] show disagreement, however, their values just fall outside of the 2-sigma ellipse of mean natural linewidths, whereas somewhat recent calculations presented in Refs. [87–89] show agreement within the 1-sigma ellipse.

The individual oscillator strengths of 3C and 3D can

TABLE II. Measured natural linewidths Γ (in meV), oscillator strength f , transition rates A^{if} (in $\times 10^{13} \text{ s}^{-1}$), and lifetimes (in fs) for lines 3C and 3D in comparison with our large-CI calculations.

	Line 3C		Line 3D	
	Experiment	Theory	Experiment	Theory
Γ	20.50 ± 1.70	20.867 ± 0.026	7.70 ± 0.70	7.570 ± 0.027
f	2.17 ± 0.18	2.204 ± 0.003	0.84 ± 0.08	0.828 ± 0.003
A^{if}	3.12 ± 0.26	3.170 ± 0.004	1.17 ± 0.11	1.150 ± 0.004
τ	32.11 ± 2.68	31.54 ± 0.040	85.48 ± 7.84	86.95 ± 0.310

be derived from the natural linewidth using the relation $f_{fi}^{\text{exp}} = C \lambda_{if}^2 (g_i/g_f) (\Gamma_{\text{exp}}/\hbar)$, where $C = 1/(32\pi^3 \alpha a_0^2 R_y) = 1.49919 \times 10^{-14} \text{ nm}^{-2}\text{s}$. g_i and g_f represent the statistical weights of the initial (i) and final states (f), respectively. The λ_{if} is the transition wavelength given in nanometers taken from [75], and \hbar is the reduced Planck constant. Moreover, the experimental lifetime and transition rates can also be derived from the natural linewidth measurements. All of these measured quantities agree very well with our predictions, given in Tab. II.

Our present experimental validation of oscillator strengths effectively eliminates uncertainties in atomic data as potential contributors to the observed discrepancies in nickel opacity measurements [40] and iron opacity [31, 41, 42]. The measured oscillator strengths offer direct application in astrophysical modeling, enabling the diagnosis of turbulent velocity in moderately optically thick plasmas [101, 102]. Upon comparing with oscillator strength ratios and natural linewidths from established databases such as NIST-ASD [92], AtomDB [93], Chianti [94], and SPEX [95], significant discrepancies were identified with our experimental results. There is a pressing need for updating these databases with such precise measurements in view of the crucial role of accurate data in modeling observational spectra from existing missions like *Chandra* and *XMM-Newton*, as well as upcoming observations with *XRISM* [103], which has recently been successfully launched, as well as future planned missions such as *Athena* [104], *LEM* [105], *HUBS* [106], *Arcus* [107], *HiReX* [108], and *Lynx* [109]. The present combination of experimental benchmark and converged calculations is a crucial consistency check for atomic data required to interpret X-ray observations in astrophysics, fusion, and high-energy density plasma research.

ACKNOWLEDGMENTS

This research was funded by the Max Planck Society (MPG) and the German Federal Ministry of Education and Research (BMBF) under project 05K13SJ2. C.S. acknowledges support from MPG and NASA under grant number 80GSFC21M0002. F.S.P. and M.A.L. acknowledge support from the NASA Astrophysics Program. The theoretical work has been supported by the US NSF Grant No. PHY-2012068, No. PHY-2309254, US Office of Naval Research Grant No. N00014-20-1-2513, and by the European Research Council (ERC) under the Horizon 2020 Research and Innovation Programme of the European Union (Grant Agreement No. 856415). Calculations were performed in part using the computing resources at the University of Delaware, in particular the Caviness and DARWIN high-performance computing clusters. We acknowledge DESY (Hamburg, Germany), a member of the Helmholtz Association HGF, for the provision of experimental facilities. Parts of this research were carried out at PETRA III. We thank Jens Viehhaus and Rolf Follath for valuable discussions on X-ray monochromator resolution and performance, and the synchrotron-operation team and P04 team at PETRA III for their skillful and reliable work. MSS

thanks MPIK, Heidelberg for hospitality.

Appendix: Theory

The calculations are carried out using a large-scale configuration interaction (CI) method [90], including correlations from all ten electrons. Basis sets of increasing sizes are used to check for convergence of the values. The basis set is designated by the highest principal quantum number for each partial wave included. For example, [12*spdfg*] means that all orbitals up to $n = 12$ are included for the *spdfg* partial waves. We begin by considering all possible single and double excitations to orbitals up to 5*spdfg* from the $2s^2 2p^6$, $2s^2 2p^5 3p$ even and $2s^2 2p^5 3s$, $2s^2 2p^5 3d$, $2s 2p^6 3p$ odd configurations, correlating 8 electrons. We verified that inclusion of the $2s 2p^6 3s$ even and $2s^2 2p^5 4s$, $2s^2 2p^5 4d$ odd configurations as basic configurations has a negligible effect on the energies and relevant matrix elements. The calculated contributions to the energies of Ni XIX are listed in Tab. III. The results are compared with a revised analysis of the experimental data [110]. We use *jj*-coupling and NIST-style LS-coupling term designations for comparisons. Contributions to the $E1$ reduced matrix elements $D(3D)$ and $D(3C)$ and the $3C/3D$ oscillator strengths ratios are listed in Table IV. The $E(3C/3D)$ energy ratio is 1.018 and the $f(3C/3D)$ oscillator strength ratio is 2.64(2).

To assess the impact of triple excitations, we consider a broad range of configurations up to 5*spdfg*. As demonstrated in Tables III and IV, these excitations result in negligible corrections to both energies and matrix elements. Subsequently, we expand the basis set to [12*spdfg*], leading to a significant improvement in the agreement of energies with experimental values and a minimal shift in the ratio (-0.008). Further accounting of contributions from the $1s^2$ shell with the [12*spdfg*] basis improves agreement with experimental energies, albeit with a marginal contribution to the $3C/3D$ ratio (-0.006). A comparison of results for $D(3C)$ and $D(3D)$ obtained in length and velocity gauges reveals only a marginal difference of 0.001 for the [12*spdfg*] basis. Expanding the basis set to [17*spdfg*] produces a modest improvement in energies compared to experiment, accompanied by a slight shift in the ratio (-0.001). Further expansion to [22*spdfg*] results in minor corrections to energies, with an even smaller contribution to the ratio (-0.0005). The quantum electrodynamic (QED) contributions are included following Ref. [111]. The QED inclusion has small effect on the individual line energies, however, a considerable contribution to the energy difference of 3C and 3D, see Tab. III. Furthermore, the ratio is changed by -0.01 by accounting for QED.

Additionally, we compute the transition rates for all other transitions contributing to the radiative decay of the 3C and 3D levels. The sums of these rates are small and listed in Tab. IV. Linewidth values correspond to total transition rates, with uncertainties computed from the largest uncertainties in the 3C and 3D matrix elements, including additional configurations in CI space and QED. Additional uncertainties due to h orbitals for transition rates and linewidths, based on recent

studies of Fe^{16+} [77], are included, and the final uncertainties are computed based on the relative difference.

-
- [1] J. Parkinson, *Astron. Astrophys.* **24**, 215 (1973).
- [2] B. W. Smith, J. B. Mann, R. D. Cowan, and J. C. Raymond, *Astrophys. J.* **298**, 898 (1985).
- [3] J. T. Schmelz, J. L. R. Saba, and K. T. Strong, *Astrophys. J. Lett.* **398**, L115 (1992).
- [4] K. Waljeski, D. Moses, K. P. Dere, J. L. R. Saba, K. T. Strong, D. F. Webb, and D. M. Zarro, *Astrophys. J.* **429**, 909 (1994).
- [5] K. J. H. Phillips, C. J. Greer, A. K. Bhatia, and F. P. Keenan, *Astrophys. J. Lett.* **469**, L57 (1996).
- [6] C. W. Mauche, D. A. Liedahl, and K. B. Fournier, *Astrophys. J.* **560**, 992 (2001), [arXiv:astro-ph/0106518 \[astro-ph\]](#).
- [7] E. Behar, J. Cottam, and S. Kahn, *Astrophys. J.* **548**, 966 (2001).
- [8] R. Doron and E. Behar, *Astrophys. J.* **574**, 518 (2002).
- [9] H. Xu, S. M. Kahn, J. R. Peterson, E. Behar, F. B. S. Paerels, R. F. Mushotzky, J. G. Jernigan, A. C. Brinkman, and K. Makishima, *Astrophys. J.* **579**, 600 (2002).
- [10] M. F. Gu, *Astrophys. J.* **582**, 1241 (2003).
- [11] F. B. S. Paerels and S. M. Kahn, *Annu. Rev. Astron. Astrophys.* **41**, 291 (2003).
- [12] A. Pradhan and S. Nahar, *Atomic astrophysics and spectroscopy* (Cambridge University Press, 2011).
- [13] P. Beiersdorfer, N. Hell, and J. Lepson, *Astrophys. J.* **864**, 24 (2018).
- [14] L. Gu, A. J. J. Raassen, J. Mao, J. de Plaa, C. Shah, C. Pinto, N. Werner, A. Simionescu, F. Mernier, and J. S. Kaastra, *Astron. Astrophys.* **627**, A51 (2019), [arXiv:1905.07871 \[astro-ph.HE\]](#).
- [15] L. Gu, C. Shah, J. Mao, T. Raassen, J. de Plaa, C. Pinto, H. Akamatsu, N. Werner, A. Simionescu, F. Mernier, M. Sawada, P. Mohanty, P. Amaro, M. F. Gu, F. S. Porter, J. R. Crespo López-Urrutia, and J. S. Kaastra, *Astron. Astrophys.* **641**, A93 (2020), [arXiv:2007.03843 \[astro-ph.HE\]](#).
- [16] G. J. Grell, M. A. Leutenegger, and C. Shah, *Astrophys. J.* **917**, 105 (2021).
- [17] G. Brown, *Can. J. Phys.* **86**, 199 (2008).
- [18] G. Brown, P. Beiersdorfer, D. Liedahl, K. Widmann, and S. Kahn, *Astrophys. J.* **502**, 1015 (1998).
- [19] G. Brown, P. Beiersdorfer, H. Chen, M. Chen, and K. Reed, *Astrophys. J. Lett.* **557**, L75 (2001).
- [20] G. Brown, P. Beiersdorfer, and K. Widmann, *Phys. Rev. A* **63**, 032719 (2001).
- [21] G. V. Brown, P. Beiersdorfer, H. Chen, J. H. Scofield, K. R. Boyce, R. L. Kelley, C. A. Kilbourne, F. S. Porter, M. F. Gu, S. M. Kahn, and A. E. Szymkowiak, *Phys. Rev. Lett.* **96**, 253201 (2006).
- [22] P. Beiersdorfer, E. Behar, K. Boyce, G. Brown, H. Chen, K. Gendreau, M. Gu, J. Gygas, S. Kahn, R. Kelley, *et al.*, *Astrophys. J. Lett.* **576**, L169 (2002).
- [23] J. Gillaspay, T. Lin, L. Tedesco, J. N. Tan, J. M. Pomeroy, J. Laming, N. Brickhouse, G.-X. Chen, and E. Silver, *Astrophys. J.* **728**, 132 (2011).
- [24] P. Beiersdorfer, M. Bitter, S. Von Goeler, and K. Hill, *Astrophys. J.* **610**, 616 (2004).
- [25] P. Beiersdorfer, J. K. Lepson, M. F. Gu, and M. Bitter, *Astrophys. J.* **850**, 57 (2017).
- [26] C. Shah, J. R. Crespo López-Urrutia, M. F. Gu, T. Pfeifer, J. Marques, F. Grilo, J. P. Santos, and P. Amaro, *Astrophys. J.* **881**, 100 (2019).
- [27] S. Bernitt, G. V. Brown, J. K. Rudolph, R. Steinbrügge, A. Graf, M. Leutenegger, S. W. Epp, S. Eberle, K. Kubiček, V. Mäkel, M. C. Simon, E. Träbert, E. W. Magee, C. Beilmann, N. Hell, S. Schippers, A. Müller, S. M. Kahn, A. Surzhykov, Z. Harman, C. H. Keitel, J. Clementson, F. S. Porter, W. Schlotter, J. J. Turner, J. Ullrich, P. Beiersdorfer, and J. R. Crespo López-Urrutia, *Nature* **492**, 225 (2012).
- [28] N. S. Oreshkina, S. M. Cavaletto, C. H. Keitel, and Z. Harman, *Phys. Rev. Lett.* **113**, 143001 (2014).
- [29] S. D. Loch, C. P. Ballance, Y. Li, M. Fogle, and C. J. Fontes, *Astrophys. J.* **801**, L13 (2015).
- [30] S. Kühn, C. Shah, J. R. Crespo López-Urrutia, K. Fujii, R. Steinbrügge, J. Stierhof, M. Togawa, Z. Harman, N. S. Oreshkina, C. Cheung, M. G. Kozlov, S. G. Porsev, M. S. Safronova, J. C. Berengut, M. Rosner, M. Bissinger, R. Ballhausen, N. Hell, S. Park, M. Chung, M. Hoesch, J. Seltmann, A. S. Surzhykov, V. A. Yerokhin, J. Wilms, F. S. Porter, T. Stöhlker, C. H. Keitel, T. Pfeifer, G. V. Brown, M. A. Leutenegger, and S. Bernitt, *Phys. Rev. Lett.* **124**, 225001 (2020).
- [31] S. Kühn, C. Cheung, N. S. Oreshkina, R. Steinbrügge, M. Togawa, S. Bernitt, L. Berger, J. Buck, M. Hoesch, J. Seltmann, F. Trinter, C. H. Keitel, M. G. Kozlov, S. G. Porsev, M. F. Gu, F. S. Porter, T. Pfeifer, M. A. Leutenegger, Z. Harman, M. S. Safronova, J. R. C. López-Urrutia, and C. Shah, *Phys. Rev. Lett.* **129**, 245001 (2022), [arXiv:2201.09070 \[physics.atom-ph\]](#).
- [32] C. Wu and X. Gao, *Scientific Reports* **9**, 7463 (2019).
- [33] G. V. Brown, P. Beiersdorfer, and K. Widmann, *Phys. Rev. A* **63**, 032719 (2001).
- [34] M. Loulergue and H. Nussbaumer, *Astron. Astrophys.* **45**, 125 (1975).
- [35] R. J. Hutcheon, J. P. Pye, and K. D. Evans, *Sol. Phys.* **46**, 171 (1976).
- [36] M. F. Gu, P. Beiersdorfer, G. V. Brown, H. Chen, K. R. Boyce, R. L. Kelley, C. A. Kilbourne, F. S. Porter, and S. M. Kahn, *Astrophys. J. Lett.* **607**, L143 (2004).
- [37] F. J. Rogers and C. A. Iglesias, *Science* **263**, 50 (1994).
- [38] M. J. Seaton, Y. Yan, D. Mihalas, and A. K. Pradhan, *Mon. Not. R. Astron. Soc.* **266**, 805 (1994).
- [39] P. Beiersdorfer, A. L. Osterheld, V. Decaux, and K. Widmann, *Phys. Rev. Lett.* **77**, 5353 (1996).
- [40] T. Nagayama, J. E. Bailey, G. P. Loisel, G. S. Dunham, G. A. Rochau, C. Blancard, J. Colgan, P. Cossé, G. Faussurier, C. J. Fontes, *et al.*, *Phys. Rev. Lett.* **122**, 235001 (2019).
- [41] J. E. Bailey, G. A. Rochau, C. A. Iglesias, J. Abdallah, J. J. MacFarlane, I. Golovkin, P. Wang, R. C. Mancini, P. W. Lake, T. C. Moore, *et al.*, *Phys. Rev. Lett.* **99**, 265002 (2007).
- [42] C. Fontes, C. Fryer, A. Hungerford, P. Hakel, J. Colgan, D. Kilcrease, and M. Sherrill, *High Energy Density Phys* **16**, 53 (2015).
- [43] H. D. Betz, F. Bell, H. Panke, G. Kalkoffen, M. Welz, and D. Evers, *Phys. Rev. Lett.* **33**, 807 (1974).
- [44] E. Träbert, *Physica Scripta* **2005**, 56 (2005).
- [45] E. Träbert, *Journal of Physics B: Atomic, Molecular and Optical Physics* **43**, 074034 (2010).
- [46] D. P. Moehs, D. A. Church, M. I. Bhatti, and W. F. Perger,

TABLE III. Contributions to the energies of Ni^{18+} calculated with increased size basis sets and number of configurations. The results are compared with a revised analysis of the experimental data [110]. All energies are given in cm^{-1} with exception of the last line that shows the difference of the 3C and 3D energies in eV. The basis set is designated by the highest quantum number for each partial wave included. For example, [12spdfg] means that all orbitals up to $n = 12$ are included for *spdfg* partial waves. Contributions from larger basis sets [17spdfg] and [22spdfg], triple excitations, excitations from the $1s^2$ shells, and QED contributions are given separately.

Configuration	J	Expt. [110]	[5spdf6g]	Triples	+ [12spdfg]	$1s^2$	+ [17spdfg]	+ [22spdfg]	QED	Final	Diff. [110]	Diff. [110]	
$2p^6$	1S	0	0	0	0	0	0	0	0	0	0		
$2p^53p$	$(3/2, 1/2)$	1	7381990	7374679	-206	3579	351	797	372	44	7379615	2375	0.03%
$2p^53p$	$(3/2, 1/2)$	2	7409915	7403138	-2	2880	264	724	331	29	7407364	2551	0.03%
$2p^53p$	$(3/2, 3/2)$	3	7431735	7424692	-4	3023	261	738	340	102	7429152	2583	0.03%
$2p^53p$	$(3/2, 3/2)$	1	7440050	7433248	-11	2836	277	730	332	85	7437497	2553	0.03%
$2p^53s$	$(3/2, 1/2)^o$	2	7105260	7096413	17	3417	478	751	350	1052	7102477	2783	0.04%
$2p^53s$	$(3/2, 1/2)^o$	1	7122600	7114019	15	3303	415	722	337	1052	7119862	2738	0.04%
$2p^53s$	$(1/2, 1/2)^o$	1	7247700	7249597	14	3386	498	735	345	1403	7255978	-8278	0.11%
$2p^53d$	$(3/2, 3/2)^o$	1	7807700	7801245	19	2336	409	684	363	72	7805128	2572	0.03%
$2p^53d$	$(3/2, 5/2)^o$	2	7825770	7819486	19	1839	415	651	359	87	7822856	2914	0.04%
$2p^53d$	$(3/2, 5/2)^o$	4	7825280	7819623	19	2044	410	677	362	88	7823223	2057	0.03%
$2p^53d$	$(3/2, 3/2)^o$	3	7830930	7825368	17	1687	414	633	353	81	7828554	2376	0.03%
$2p^53d$	$(3/2, 3/2)^o$	2	7847100	7841657	18	1638	410	654	356	86	7844819	2281	0.03%
$2p^53d$	$(3/2, 5/2)^o$	3	7857640	7852407	17	1705	407	630	350	90	7855606	2034	0.04%
$2p^53d$	$(3/2, 5/2)^o$	1	7901400	7899252	3	1681	384	638	352	136	7902446	-1046	0.01%
$2p^53d$	$(1/2, 3/2)^o$	2	7972475	7967013	17	1683	484	657	362	432	7970647	1828	0.02%
$2p^53d$	$(1/2, 5/2)^o$	2	7980810	7975017	17	1933	475	667	362	427	7978897	1913	0.02%
$2p^53d$	$(1/2, 5/2)^o$	3	7986640	7981013	16	1759	481	638	356	443	7984706	1934	0.02%
$2p^53d$	$(1/2, 3/2)^o$	1	8041800	8040754	-29	1668	383	633	353	372	8044132	-2332	0.03%
$3C - 3D$	(eV)		17.4074	17.5440	-0.0039	-0.0016	-0.0002	-0.0006	-0.0001	0.0291	17.5669		

TABLE IV. Contributions to the E1 reduced matrix elements $D(3D) = D(2p^6 \ ^1S_0 - 2p^5 3d \ (3/2, 5/2))$ and $D(3C) = D(2p^6 \ ^1S_0 - 2p^5 3d \ (1/2, 3/2))$ (in a.u.) and the ratio of the respective oscillator strengths R in Ni^{18+} . See caption of Table III for designations. L and V rows compared results obtained in length and velocity gauges for the [12spdfg] basis. All other results are calculated using the length gauge. Transition rates and linewidth are listed at the bottom of the table. Total of the other transition rates contributing to the lifetime of the 3C and 3D levels are listed in row “Other transitions”.

		$D(3C)$	$\Delta D(3C)$	$D(3D)$	$\Delta D(3D)$	$R(3C/3D)$	ΔR
[5 <i>spdf</i> 6 <i>g</i>]		0.30012		0.18530		2.670	
	+Triples	0.29999	-0.00013	0.18530	0.00000	2.668	-0.002
[12 <i>spdfg</i>]	L	0.30031	0.00019	0.18568	0.00038	2.662	-0.008
	V	0.30060		0.18582		2.663	
[12 <i>spdfg</i>]	+1 <i>s</i> ²	0.30018	-0.00013	0.18581	0.00013	2.656	-0.006
[17 <i>spdfg</i>]		0.30032	0.00001	0.18571	0.00003	2.662	-0.001
[22 <i>spdfg</i>]		0.30031	-0.00001	0.18572	0.00001	2.661	-0.0005
QED			-0.00012		0.00028		-0.010
Final		0.29993		0.18613		2.64(2)	
Recommended transition rate (s ⁻¹)		3.168(4)×10 ¹³		1.148(4)×10 ¹³			
Other transitions (s ⁻¹)		1.75×10 ¹⁰		1.59×10 ¹⁰			
Total rate (s ⁻¹)		3.170(4)×10 ¹³		1.150(4)×10 ¹³			
Linewidth (meV)		20.867(26)		7.570(27)			

Phys. Rev. Lett. **85**, 38 (2000).

- [47] D. P. Moehs, M. I. Bhatti, and D. A. Church, *Phys. Rev. A* **63**, 032515 (2001).
 [48] S. J. Smith, A. Chutjian, and J. A. Lozano, *Phys. Rev. A* **72**, 062504 (2005).
 [49] S. Mannervik, J. Lidberg, L. O. Norlin, and P. Royen, *Phys. Rev. A* **56**, R1075 (1997).
 [50] E. Träbert, G. Gwinner, A. Wolf, E. J. Knystautas, H.-P. Garnir, and X. Tordoir, *Journal of Physics B: Atomic, Molecular*

and Optical Physics **35**, 671 (2002).

- [51] E. Träbert, *Canadian Journal of Physics* **80**, 1481 (2002), <https://doi.org/10.1139/p02-123>.
 [52] E. Träbert, A. G. Calamai, G. Gwinner, E. J. Knystautas, E. H. Pinnington, and A. Wolf, *Journal of Physics B: Atomic, Molecular and Optical Physics* **36**, 1129 (2003).
 [53] E. Träbert, G. Saathoff, and A. Wolf, *Journal of Physics B: Atomic, Molecular and Optical Physics* **37**, 945 (2004).
 [54] E. Träbert, S. Reinhardt, J. Hoffmann, and A. Wolf, *Journal*

- of Physics B: Atomic, Molecular and Optical Physics **39**, 945 (2006).
- [55] E. Träbert, M. Grieser, J. Hoffmann, C. Krantz, R. Repnow, and A. Wolf, *Phys. Rev. A* **85**, 042508 (2012).
- [56] E. Träbert, M. Grieser, R. von Hahn, C. Krantz, R. Repnow, and A. Wolf, *New Journal of Physics* **14**, 023061 (2012).
- [57] E. Träbert, M. Grieser, C. Krantz, R. Repnow, A. Wolf, F. J. Diaz, Y. Ishikawa, and J. A. Santana, *Journal of Physics B: Atomic, Molecular and Optical Physics* **45**, 215003 (2012).
- [58] E. Träbert, *Atoms* **10**, 114 (2022).
- [59] E. Träbert, *Atoms* **11**, 85 (2023).
- [60] D. Habs, W. Baumann, J. Berger, P. Blatt, A. Faulstich, P. Krause, G. Kilgus, R. Neumann, W. Petrich, R. Stokstad, *et al.*, *Nucl. Instrum. Methods Phys. Res., Sect. B* **43**, 390 (1989).
- [61] J. Doerfert, E. Träbert, A. Wolf, D. Schwalm, and O. Uwira, *Phys. Rev. Lett.* **78**, 4355 (1997).
- [62] I. KRAFT, S. Borneis, T. Engel, B. Fricke, R. Grieser, G. Huber, T. Kühl, D. Marx, R. Neumann, S. Schröder, P. Seelig, and L. Völker, *Phys. Rev. Lett.* **73**, 2425 (1994).
- [63] P. Seelig, S. Borneis, A. Dax, T. Engel, S. Faber, M. Gerlach, C. Holbrow, G. Huber, T. Kühl, D. Marx, K. Meier, P. Merz, W. Quint, F. Schmitt, M. Tomaselli, L. Völker, H. Winter, M. Würtz, K. Beckert, B. Franzke, F. Nolden, H. Reich, M. Steck, and T. Winkler, *Phys. Rev. Lett.* **81**, 4824 (1998).
- [64] M. Lochmann, R. Jöhren, C. Geppert, Z. Andelkovic, D. Anielski, B. Botermann, M. Bussmann, A. Dax, N. Frömmgen, M. Hammen, V. Hannen, T. Kühl, Y. A. Litvinov, R. López-Coto, T. Stöhlker, R. C. Thompson, J. Vollbrecht, A. Volotka, C. Weinheimer, W. Wen, E. Will, D. Winters, R. Sánchez, and W. Nörtershäuser, *Phys. Rev. A* **90**, 030501 (2014).
- [65] J. R. Crespo López-Urrutia, P. Beiersdorfer, D. W. Savin, and K. Widmann, *Phys. Rev. A* **58**, 238 (1998).
- [66] P. Beiersdorfer, E. Träbert, and E. H. Pinnington, *The Astrophysical Journal* **587**, 836 (2003).
- [67] J. R. Crespo López-Urrutia, P. Beiersdorfer, and K. Widmann, *Phys. Rev. A* **74**, 012507 (2006).
- [68] J. R. Crespo López-Urrutia and P. Beiersdorfer, *Astrophys. J.* **721**, 576 (2010).
- [69] P. Beiersdorfer, J. R. Crespo López-Urrutia, and E. Träbert, *Astrophys. J.* **817**, 67 (2016).
- [70] J. K. Rudolph, S. Bernitt, S. W. Epp, R. Steinbrügge, C. Beilmann, G. V. Brown, S. Eberle, A. Graf, Z. Harman, N. Hell, M. Leutenegger, A. Müller, K. Schlage, H.-C. Wille, H. Yavaş, J. Ullrich, and J. R. Crespo López-Urrutia, *Phys. Rev. Lett.* **111**, 103002 (2013).
- [71] R. Steinbrügge, S. Bernitt, S. W. Epp, J. K. Rudolph, C. Beilmann, H. Bekker, S. Eberle, A. Müller, O. O. Versolato, H.-C. Wille, H. Yavaş, J. Ullrich, and J. R. Crespo López-Urrutia, *Phys. Rev. A* **91**, 032502 (2015).
- [72] R. Steinbrügge, S. Kühn, F. Nicastro, M. F. Gu, M. Togawa, M. Hoesch, J. Seltmann, I. Sergeev, F. Trinter, S. Bernitt, C. Shah, M. A. Leutenegger, and J. R. Crespo López-Urrutia, *Astrophys. J.* **941**, 188 (2022).
- [73] P. Mücke, S. Kühn, L. Buchauer, J. R. Harries, T. M. Bücking, K. Blaum, A. Cieluch, A. Egl, D. Hollain, S. Kraemer, T. Pfeifer, P. O. Schmidt, R. X. Schüssler, C. Schweiger, T. Stöhlker, S. Sturm, R. N. Wolf, S. Bernitt, and J. R. Crespo López-Urrutia, *Rev. Sci. Instrum.* **89**, 063109 (2018).
- [74] J. Vieffhaus, F. Scholz, S. Deinert, L. Glaser, M. Ilchen, J. Seltmann, P. Walter, and F. Siewert, *Nucl. Instrum. Methods Phys. Res., Sect. A* **710**, 151 (2013).
- [75] M. F. Gu, P. Beiersdorfer, G. V. Brown, H. Chen, D. B. Thorn, and S. M. Kahn, *Astrophys. J.* **657**, 1172 (2007).
- [76] M. Hoesch, J. Seltmann, F. Trinter, S. Kühn, M. Togawa, R. Steinbrügge, S. Bernitt, and J. R. C. López-Urrutia, *Journal of Physics: Conference Series* **2380**, 012086 (2022).
- [77] C. Shah, M. Togawa, M. Botz, J. Danisch, J. J. Goes, S. Bernitt, M. Maxton, K. Köbnick, J. Buck, J. Seltmann, M. Hoesch, M. F. Gu, F. S. Porter, T. Pfeifer, M. A. Leutenegger, C. Cheung, M. S. Safronova, and J. R. Crespo López-Urrutia, *arXiv e-prints*, [arXiv:2401.08395](https://arxiv.org/abs/2401.08395) [physics.atom-ph].
- [78] R. Follath and A. Balzer, in *Sri 2009, 10th International Conference on Synchrotron Radiation Instrumentation*, American Institute of Physics Conference Series, Vol. 1234, edited by R. Garrett, I. Gentle, K. Nugent, and S. Wilkins (2010) pp. 657–660.
- [79] W. Cash, *Astrophys. J.* **228**, 939 (1979).
- [80] J. S. Kaastra, *Astron. Astrophys.* **605**, A51 (2017), [arXiv:1707.09202](https://arxiv.org/abs/1707.09202) [astro-ph.HE].
- [81] E. Träbert, *Atoms* **10**, 10.3390/atoms10020046 (2022).
- [82] M. Gu, P. Beiersdorfer, G. Brown, H. Chen, K. Boyce, R. Kelley, C. Kilbourne, F. Porter, and S. Kahn, *Astrophys. J. Lett.* **607**, L143 (2004).
- [83] G. X. Chen, K. Kirby, E. Silver, N. S. Brickhouse, J. D. Gillaspay, J. N. Tan, J. M. Pomeroy, and J. M. Laming, *Phys. Rev. Lett.* **97**, 143201 (2006).
- [84] D. McKenzie, P. Landecker, R. Broussard, H. Rugge, R. Young, U. Feldman, and G. Doschek, *Astrophys. J.* **241**, 409 (1980).
- [85] H. L. Zhang and D. Sampson, *At. Data Nucl. Data Tables* **43**, 1 (1989).
- [86] U. I. Safronova, C. Namba, I. Murakami, W. R. Johnson, and M. S. Safronova, *Phys. Rev. A* **64**, 012507 (2001).
- [87] C. Dong, L. Xie, S. Fritzsche, and T. Kato, *Nucl. Instrum. Methods Phys. Res., Sect. B* **205**, 87 (2003), 11th International Conference on the Physics of Highly Charged Ions.
- [88] P. Jönsson, P. Bengtsson, J. Ekman, S. Gustafsson, L. B. Karlsson, G. Gaigalas, C. F. Fischer, D. Kato, I. Murakami, H. A. Sakaue, H. Hara, T. Watanabe, N. Nakamura, and N. Yamamoto, *At. Data Nucl. Data Tables* **100**, 1 (2014).
- [89] J. A. Santana, J. K. Lepson, E. Träbert, and P. Beiersdorfer, *Phys. Rev. A* **91**, 012502 (2015).
- [90] C. Cheung, M. Safronova, and S. Porsev, *Symmetry* **13**, 10.3390/sym13040621 (2021).
- [91] M. F. Gu, *Can. J. Phys.* **86**, 675 (2008).
- [92] A. Kramida, Yu. Ralchenko, J. Reader, and NIST ASD Team, NIST Atomic Spectra Database (ver. 5.9), [Online]. Available: <https://physics.nist.gov/asd> [Mon Jun 20 2022]. National Institute of Standards and Technology, Gaithersburg, MD. (2022).
- [93] A. R. Foster, L. Ji, R. K. Smith, and N. S. Brickhouse, *Astrophys. J.* **756**, 128 (2012).
- [94] G. Del Zanna and Y. Ishikawa, *Astron. Astrophys.* **508**, 1517 (2009).
- [95] J. S. Kaastra, R. Mewe, and H. Nieuwenhuijzen, in *UV and X-ray Spectroscopy of Astrophysical and Laboratory Plasmas* (1996) pp. 411–414.
- [96] J. Krempaský, R. Follath, V. N. Strocov, T. Schmitt, and U. Flechsig, in *Society of Photo-Optical Instrumentation Engineers (SPIE) Conference Series*, Society of Photo-Optical Instrumentation Engineers (SPIE) Conference Series, Vol. 8139 (2011) p. 81390K.
- [97] M. Togawa, S. Kühn, C. Shah, and Others, *Untitled manuscript*, Under Review (2023).
- [98] K. Rossnagel, L. Kipp, M. Skibowski, and S. Harm, *Nucl. In-*

- strum. *Methods Phys. Res., Sect. A* **467-468**, 1485 (2001), proceedings of the 7th Int. Conf. on Synchrotron Radiation Instrumentation.
- [99] N. M. Cann and A. J. Thakkar, *Phys. Rev. A* **46**, 5397 (1992).
- [100] W. R. Johnson, I. M. Savukov, U. I. Safronova, and A. Dalgarno, *The Astrophysical Journal Supplement Series* **141**, 543 (2002).
- [101] H. Xu, S. Kahn, J. Peterson, E. Behar, F. Paerels, R. Mushotzky, J. Jernigan, A. Brinkman, and K. Makishima, *Astrophys. J.* **579**, 600 (2002).
- [102] N. Werner, I. Zhuravleva, E. Churazov, A. Simionescu, S. W. Allen, W. Forman, C. Jones, and J. Kaastra, *Mon. Not. R. Astron. Soc.* **398**, 23 (2009).
- [103] M. Tashiro, H. Maejima, K. Toda, R. Kelley, L. Reichenthal, J. Lobell, R. Petre, M. Guainazzi, E. Costantini, M. Edison, *et al.*, *Proc. SPIE* **10699**, 1069922 (2018).
- [104] F. Pajot, D. Barret, T. Lam-Trong, J.-W. Den Herder, L. Piro, M. Cappi, J. Huvelin, R. Kelley, J. Mas-Hesse, K. Mitsuda, *et al.*, *J. Low Temp. Phys.* **193**, 901 (2018).
- [105] R. Kraft, M. Markevitch, C. Kilbourne, J. S. Adams, H. Akamatsu, M. Ayromlou, S. R. Bandler, M. Barbera, D. A. Bennett, A. Bhardwaj, V. Biffi, D. Bodewits, A. Bogdan, M. Bonamente, S. Borgani, G. Branduardi-Raymont, J. N. Bregman, J. N. Burchett, J. Cann, J. Carter, P. Chakraborty, E. Churazov, R. A. Crain, R. Cumbee, R. Dave, M. DiPirro, K. Dolag, W. Bertrand Doriese, J. Drake, W. Dunn, M. Eckart, D. Eckert, S. Etori, W. Forman, M. Galeazzi, A. Gall, E. Gatzuz, N. Hell, E. Hodges-Kluck, C. Jackman, A. Jahromi, F. Jennings, C. Jones, P. Kaaret, P. J. Kavanagh, R. L. Kelley, I. Khabibullin, C.-G. Kim, D. Koutroumpa, O. Kovacs, K. D. Kuntz, E. Lau, S.-H. Lee, M. Leutenegger, S.-C. Lin, C. Lisse, U. Lo Cicero, L. Lovisari, D. McCammon, S. McEntee, F. Mernier, E. D. Miller, D. Nagai, M. Negro, D. Nelson, J.-U. Ness, P. Nulsen, A. Ogorzalek, B. D. Oppenheimer, L. Oskionova, D. Patnaude, R. W. Pfeifle, A. Pillepich, P. Plucinsky, D. Pooley, F. S. Porter, S. Randall, E. Rasia, J. Raymond, M. Ruszkowski, K. Sakai, A. Sarkar, M. Sasaki, K. Sato, G. Schellenberger, J. Schaye, A. Simionescu, S. J. Smith, J. F. Steiner, J. Stern, Y. Su, M. Sun, G. Tremblay, N. Truong, J. Tutt, E. Ursino, S. Veilleux, A. Vikhlinin, S. Vladutescu-Zopp, M. Vogelsberger, S. A. Walker, K. Weaver, D. M. Weigt, J. Werk, N. Werner, S. J. Wolk, C. Zhang, W. W. Zhang, I. Zhuravleva, and J. ZuHone, *arXiv e-prints*, [arXiv:2211.09827](https://arxiv.org/abs/2211.09827) (2022), [arXiv:2211.09827](https://arxiv.org/abs/2211.09827) [astro-ph.IM].
- [106] W. Cui, L. B. Chen, B. Gao, F. L. Guo, H. Jin, G. L. Wang, L. Wang, J. J. Wang, W. Wang, Z. S. Wang, Z. Wang, F. Yuan, and W. Zhang, *Journal of Low Temperature Physics* **199**, 502 (2020).
- [107] R. K. Heilmann, A. R. Brucoleri, V. Burwitz, C. DeRoo, A. Garner, H. M. Günther, E. M. Gullikson, G. Hartner, E. Hertz, A. Langmeier, T. Müller, S. Rukdee, T. Schmidt, R. K. Smith, and M. L. Schattenburg, *Astrophys. J.* **934**, 171 (2022), [arXiv:2206.09013](https://arxiv.org/abs/2206.09013) [astro-ph.IM].
- [108] F. Nicastro, J. Kaastra, C. Argiroffi, E. Behar, S. Bianchi, F. Bocchino, S. Borgani, G. Branduardi-Raymont, J. Bregman, E. Churazov, M. Diaz-Trigo, C. Done, J. Drake, T. Fang, N. Grosso, A. Luminari, M. Mehdipour, F. Paerels, E. Piconcelli, C. Pinto, D. Porquet, J. Reeves, J. Schaye, S. Sciortino, R. Smith, D. Spiga, R. Tomaru, F. Tombesi, N. Wijers, and L. Zappacosta, *Experimental Astronomy* **51**, 1013 (2021).
- [109] D. A. Schwartz, A. Vikhlinin, H. Tananbaum, M. Freeman, G. Tremblay, E. D. Schwartz, J. A. Gaskin, D. Swartz, K. Gelmis, K. S. McCarley, and A. Dominguez, in *UV, X-Ray, and Gamma-Ray Space Instrumentation for Astronomy XXI*, Society of Photo-Optical Instrumentation Engineers (SPIE) Conference Series, Vol. 11118, edited by O. H. Siegmund (2019) p. 111180K.
- [110] A. Kramida, Personal Communication (2019).
- [111] I. I. Tupitsyn, M. G. Kozlov, M. S. Safronova, V. M. Shabaev, and V. A. Dzuba, *Phys. Rev. Lett.* **117**, 253001 (2016).